Membrane potential as master regulator of cellular mechano-transduction

Avik Mukherjee*, Yanqing Huang*, Jens Elgeti, Seungeun Oh, Jose G. Abreu Jr., Anjali Rebecca Neliat, Janik Schüttler, Dan-Dan Su, Nina Catherine Benites, Xili Liu, Leonid Peshkin, Mihail Barboiu, Hugo Stocker, Marc W. Kirschner, Markus Basan[#]

[#] Correspondence: markus@hms.harvard.edu **,** *equal contribution

The establishment of membrane potential is a property of all living cells[1]. Nevertheless, its physiological role in non-excitable cells is poorly understood. Resting membrane potential is typically considered fixed for a given cell type and under tight homeostatic control[2]. Contrary to this widely accepted opinion, we found that membrane potential can be a dynamic property that reflects mechanical forces acting on the cell. We show that important mechano-sensing pathways, like YAP, JNK and p38[3–7], are directly controlled by membrane potential. Moreover, we show that mechano-transduction via membrane potential plays a critical role in the homeostasis of epithelial tissues, setting cellular biomass density and cell number density by controlling proliferation and cell elimination. We find that mechanical stretching results in a wave of depolarization during wound healing that enhances the efficiency of wound closure. Together these data are explained by a biophysical model that demonstrates that membrane potential is physically coupled to mechanical pressure and cellular biomass density, thereby providing a quasi-instantaneous, global readout of the biophysical state of the cell. Membrane potential in turn regulates cell growth, resulting in homeostatic feedback control of biomass density and cell number density in tissues. Mechano-transduction via membrane potential may be an ancient homeostatic mechanism for cell density, cell size and growth control in multi-cellular organisms and its misregulation may play a role in tumorigenesis.

How the volume, mass and macromolecule density of metazoan cells are regulated is poorly understood but critical for biochemical functions at cellular level, as well as for the growth and homeostasis of tissues and organisms. Most reviews propose or assume that biomass density is constant, so cell mass and volume are inversely proportional. We tested this assumption in epithelial monolayers in culture, which are thought to model the properties of real epithelia in tissues[8]. We used normalized Raman imaging (NoRI)[9] to quantify the intracellular biomass density of epithelial MDCK monolayers at increasing levels of confluence (Fig. 1a, Fig. S1). Remarkably, rather than remaining constant, as might intuitively be expected, the density underwent a striking increase as a function of the increased cell density. We confirmed this observation with a second independent microscopic technique, based on laser interferometry, also referred to as holo-tomographic microscopy (Tomocube) (Fig. 1a, red squares & Fig. S2)[10,11].

Tissue density is reflected in membrane potential

Inspired by physical phenomena from equilibrium thermodynamics[12], we wanted to know whether changes in biomass density were reflected in changes of membrane potential. Using the hybrid voltage-indicator Voltron[13], we quantified the membrane potential in MDCK cells as a function of cell number and biomass density. Strikingly, MDCK cells became increasingly hyperpolarized with increasing cell number (Fig. 1b). This finding is surprising because membrane potential is typically considered to be under tight homeostatic control and constant for a given cell type. Nevertheless, this finding in MDCK cells was consistent with early glass-microelectrode ~~micropipette~~-based measurements of the resting membrane potential in CHO cells as they reached different levels confluence and in different regions of the colony[14](Fig. S3a,b,d). Similarly, our measurements in different regions of CHO colonies showed increasing depolarization with decreasing cell number density (Fig. S3e). The mechanistic basis or consequence of these early observations has never been explained. We hypothesized that, just like in MDCK cells, changes in CHO cells' membrane potential might correlate with changes in cellular biomass density. Indeed, using NoRI imaging, we confirmed that in CHO cells, changes in membrane potential were accompanied by corresponding changes in cellular biomass density (Fig. S3c, e), with denser cells being more negatively polarized. Unlike MDCK, CHO cells do not form a tight epithelium connected by tight junctions, suggesting the relationship between membrane potential and biomass density is general.

The correlation of biomass density and membrane potential suggested that these physiological variables are directly coupled. To test the causal nature of this relationship, we applied external osmotic pressure to compress cells, artificially increasing their biomass density, and assayed the resulting membrane potential. Indeed, we confirmed that both CHO cells and MDCK cells were hyperpolarized by osmotic compression (Fig. S4), suggesting that changes in membrane potential may be a result of changes in biomass density.

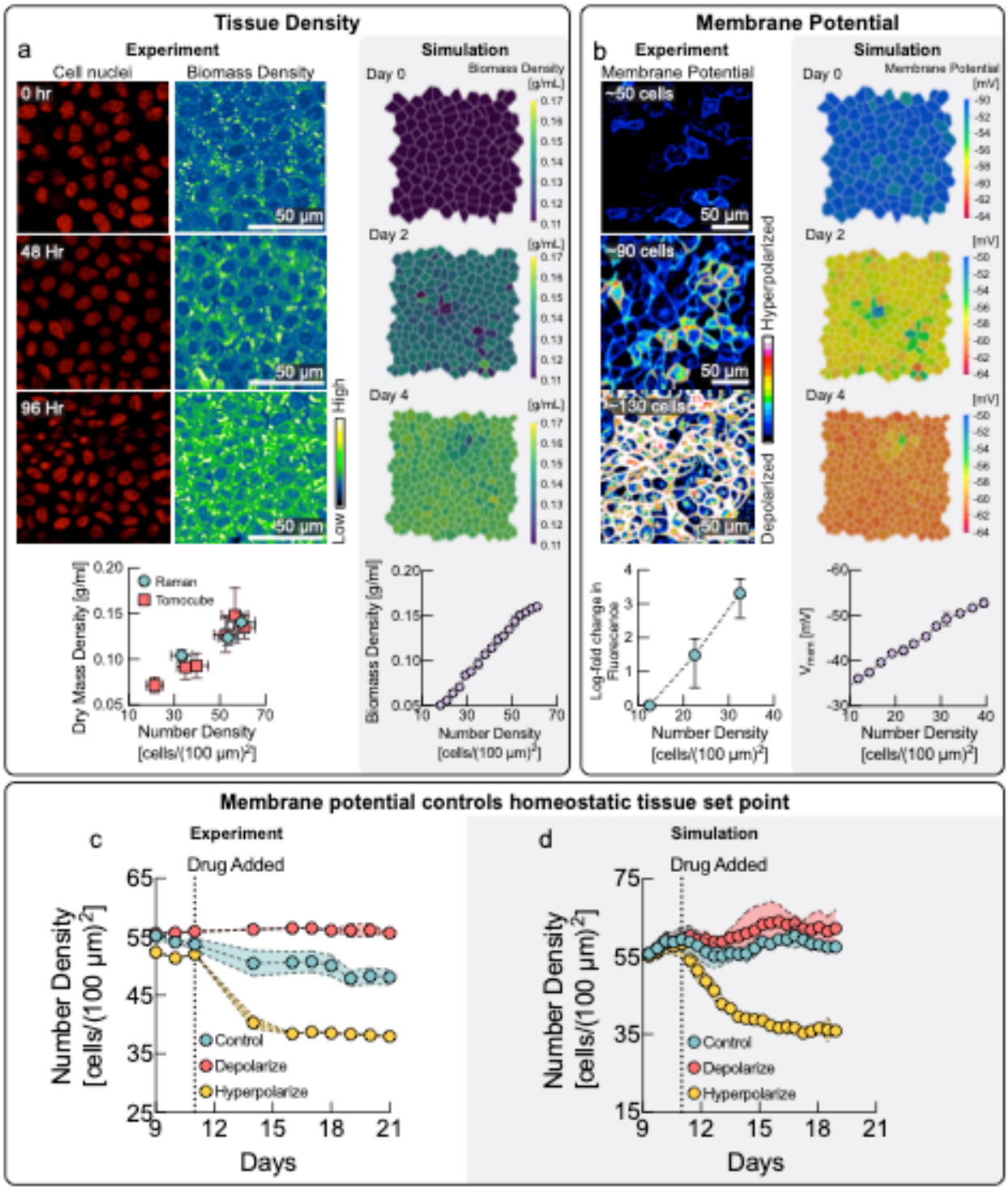

Figure 1: Membrane potential is a sensor and regulator of tissue density. a*, Madin-Darby Canine Kidney (MDCK) cells imaged for 4 consecutive days after confluence with increasing cell number density. Left row of images shows number of cell nuclei and middle row of images shows cellular biomass density (in units of g/ml) measured via Normalized Stimulated Raman Spectroscopy (NoRI). Plot below shows cellular biomass density quantified as a function of cell number density in the tissue. Biomass density was measured using two different experimental methods (NoRI imaging and holotomographic microscopy). Right row of images are snapshots*

of the tissue simulation with biomass density represented by the color code. Plot below displays corresponding biomass density as a function of cell number density from the tissue simulation. (NoRI imaging: each point represents the average of 15 measurements, error bars represent SD, 5 cells quantified from 3 images from 3 biological replicates. Holotomographic imaging : each point is quantified from ~18-21 individual cells, error bars represent SD. Tissue simulation : each point represents the average of the simulated biomass density quantified from 4 independent simulations. Error bars represents SD.) ***b,*** *Left row of images shows MDCK cells, stably expressing Voltron biosensor. An increase in fluorescence intensity indicates hyperpolarization of cellular membrane potential. Cells show progressive hyperpolarization as a function of increasing cell density. Plot below is a quantification of reporter readout of membrane potential as a function of tissue density. Right row of images are snapshots of the tissue simulation (same as in panel a) with membrane potential represented by the color code. Plot below shows corresponding quantification of membrane potential as a function of tissue density in the simulation. (Biosensor imaging: n=8 cells quantified for each point, error bars represent SD. Tissue simulation: each point represents the average quantified from 4 independent simulation. Error bars represents SD.)* ***c,*** *Quantification of cell number density for MDCK cells grown to maximum tissue density and treated with depolarizing and hyperpolarizing drugs (TCT, valinomycin) as a function of time. Steady-state cell number density can be modulated by membrane potential. Depolarization results in higher tissue density (red) as compared to the control without drugs (blue). This effect was independent of the depolarizing drug used (gramicidin, TCT) (see Fig. S5). Conversely, hyperpolarization results in a substantially lower tissue density (yellow). This effect was dose dependent (see Fig. S5). In a separate experiment, we showed that depolarization of cells that had already reached maximum confluence density, resulted in a further substantial increase in cell number density, as well as cellular biomass density (see Fig. S6). (Control: average of 10 independent wells. Depolarizing and hyperpolarizing conditions: 3 independent wells. Error bars represent SD.)* ***d,*** *Results from the tissue simulation corresponding to experiment in panel c. The mechanisms of different depolarizing and hyperpolarizing drugs were implemented in the tissue simulation via the mechano-electro-osmotic model. Just as observed experimentally, depolarizing drugs result in a higher homeostatic tissue density (red), whereas hyperpolarizing drugs result in a decrease of homeostatic tissue density (yellow), as compared to the unperturbed tissue (blue). (Average cell number quantified from 4 independent simulations, error bars represent SD).*

Membrane potential regulates biomass density and cell number density

Based on these observations, we hypothesized that membrane potential could be directly involved in regulating tissue biomass density and cell number density. To test this hypothesis, we grew MDCK cells to maximum density and then applied either depolarizing (TCT[15,16]) or hyperpolarizing (valinomycin) drugs to the tissue culture. Strikingly, cells in depolarizing conditions (Fig. 1c, red symbols) maintained a significantly higher cell number density than cells grown in the absence of drugs (Fig. 1c, blue symbols). We found the effect to be independent of the depolarizing drug (gramicidin, TCT) used (Fig. S5). Conversely, the number density of cells in hyperpolarizing conditions dropped and then plateaued at a substantially lower level (Fig. 1c, yellow) than in the tissues grown in the absence of drugs (Fig. 1c, cyan). This steady-state cell number density could be modulated continuously with the dose of the hyperpolarizing drug (valinomycin) (Fig. S5), consistent with a regulatory role of membrane potential in controlling tissue density. Gramicidin and its synthetic analog TCT form channel-like pores on the

membrane. We wanted to know if we could achieve the same effect by blocking the sodium-potassium ATPase. Indeed, using the drug ouabain, we confirmed that depolarization of cells at maximum confluence density, resulted in a substantial increase of both cellular biomass density and cell number density (Fig. S6).

Mechano-electro-osmotic model

To understand how membrane potential might control biomass density and the effect of cell density on proliferation, we built a biophysical mathematical model of ion homeostasis, cellular biomass and mechanical pressure. Classical models of membrane potential do not consider mechanical forces at all, and their systems of equations are only closed by introducing unphysical simplifications[2,17]. Models correctly rooted in elementary physical laws were developed in the 1960s and showed that osmotic stabilization of cells requires constant ion export that results in a build-up of membrane potential as a by-product[18–20]. However, it remained unclear how these models should be applied to growing cells, as they change in cell mass, cell membrane and volume, and model parameters like permeability and transport activity are subject to change. More importantly, none of these works uncovered that membrane potential, a by-product of volume stabilization, may directly convey crucial physiological information to cells and direct cellular decision making.

Membrane potential is in fact intimately coupled to osmotic pressure of the cytoplasm and the balance of charged ions and macromolecules inside the cell. As illustrated in Box 1 (top), an imaginary cell resists external forces compressing it via osmotic pressure resulting from an increased concentration of intracellular macromolecules in the cytoplasm and an increased concentration of counterions. However, this results in a steeper ion concentration gradient across the plasma membrane promoting a larger efflux of ions. A buildup of membrane potential due to charged biomolecules inside the cell counteracts this diffusive efflux, retaining an elevated intracellular ion concentration to counteract the external pressure. In equilibrium conditions, this is known as the Gibbs-Donnan effect[12], but the same processes are at play far from equilibrium. With a constant expression ratio of ion transporters and channels, membrane potential constitutes a cell size-independent readout of total mechanical pressure on the cell and the corresponding cytoplasmic biomass density (see Box 1 & Supplementary Note 1). In effect, membrane potential physically controls biomass density and mechanical forces, and vice versa, but crucially it provides cells with an accessible readout of biomass density and mechanical forces for signal transduction. Of note, the polarity of the membrane potential in the model is determined by the net charge on the macromolecules in the cell. Negative charge dominates over positive because the proteome has an average isolectric point above 7[21] and nucleic acids, especially the significant fraction of the biomass in the cytoplasm comprised of RNA[22], are negatively charged. As a result, K+ and Na+ are more abundant than cations in the cytoplasm, and the membrane potential polarity is such that there is net negative charge on the inside of the cell.

Tissue simulation

We calibrated the mechano-electro-osmotic model, with physiological parameters and use it to simulate a mono-layered epithelium (Supplementary Note 2). Membrane potential provides cells in the tissue with a quasi-instantaneous readout of tissue density and the mechanical constraints, important for tissue homeostasis (Fig. 1c). Because the coupling between mechanics, density and membrane potential requires no active regulation and is present even at thermodynamic

equilibrium, we hypothesize that regulation via membrane potential could be one of the earliest homeostatic mechanisms employed in multi–cellular organisms. To test the idea that tissues can achieve homeostasis relying only on the membrane potential as a controller, we tested a model where the membrane potential is the sole regulator of biosynthesis and apoptosis (see Supplementary Note 2 for details of implementation).

Indeed, the tissue simulation successfully recapitulated our experimental observations, including the increase in biomass density with cell number density (Fig. 1a, right side) and the corresponding changes in membrane potential (Fig. 1b, right side). Implementing the mechanism of different depolarizing and hyperpolarizing drugs in the simulation, the model recapitulated the observed changes in steady-state tissue density (Fig. 1c, right side). The general effect of these drugs can be understood intuitively: Cells perceive mild depolarization to be a state of low confluence. They continue to grow generating an excessive density (Fig. 1c, red circles). Conversely, hyperpolarization by drugs leads to a lower homeostatic tissue density because cells seem to interpret hyperpolarization as excess tissue density and arrest their growth prematurely. The regulation of cell growth by membrane potential, correctly predicts changes in steady-state tissue density.

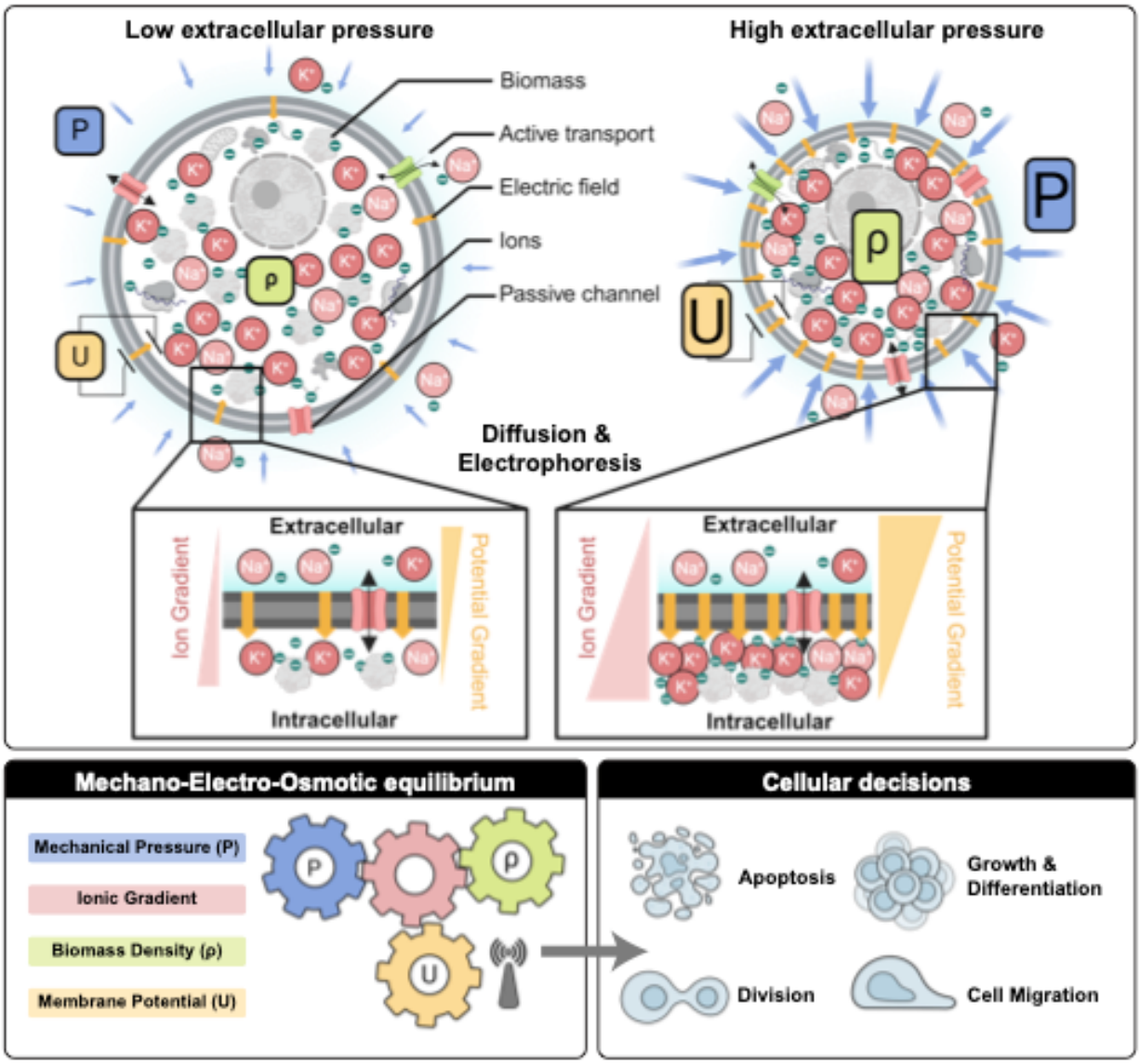

Box 1: Mechano-electro-osmotic model. Top: *The model combines three elementary conservation laws: Flux balance across the plasma membrane, mechanical force balance, and charge balance. Left-hand side illustrates a cell under low mechanical pressure and the right-hand side a corresponding cell under high mechanical pressure. Cellular biomass like protein and RNA carries a net negative charge. Cells resist compression of their volume via cytoplasmic osmotic pressure that counteracts and balances external forces (force balance). This osmotic pressure originates from an intracellular concentration of counterions that are attracted to balance negatively charged macromolecules (charge balance). As illustrated on the right-hand side, higher mechanical pressure acting in the cell is thus balanced by a higher concentration of counterions. Higher intracellular ion concentrations result in steeper concentration gradients across the membrane, as illustrated in the right inset. With constant ion channel abundances, a steeper concentration gradient across the membrane results in an augmented diffusive efflux of ions (Fick's law). With constant active ion transport flux (sodium-potassium-ATPase), this increased diffusive ion efflux results in a buildup of net negative charge in the cytoplasm and a*

corresponding membrane potential that counteracts the diffusive efflux of positively charged ions until flux balance is achieved (flux balance for each ion species). ***Bottom:*** *A one-to-one correspondence between mechanical pressure, cytoplasmic biomass density and membrane potential emerges from the mechano-electro-osmotic equilibrium illustrated in the top panel. Crucial physiological properties like total biomass in relation to available space or mechanical and spatial constraints on the entire cell are difficult for cells to assess and integrate from individual molecular players. Membrane potential, on the other hand, provides an instantaneous, global readout of these physiological variables. We hypothesize that membrane potential is therefore the ideal starting point for signal transduction to control cellular decisions like growth, apoptosis, and cell motility to achieve tissue homeostasis.*

Membrane potential reflects mechanical forces

The mechano-electro-osmotic model (Box 1) predicts that mechanical forces should be directly reflected in the membrane potential. To test this prediction, we imposed external mechanical perturbations on the tissue and measured the response of membrane potential. One method is to culture epithelial cells on an elastic membrane that can be stretched or de-stretched mechanically, thereby expanding or compressing the tissue itself[23,24] (Fig. 2a). We cultured MDCK cells on such a stretchable PDMS membrane and waited till cells reached maximum number density. We employed the voltage sensitive dye FluoVolt, whose fluorescence intensity increases with depolarization[25], as it is ideally suited to image changes in membrane potential on short timescales. Indeed, stretching the MDCK monolayer resulted in depolarization (Fig. 2a,b, quantified in panel c), consistent with simulation prediction (Fig. 2d). To check that this change in membrane potential was reversible on short timescales when we de-stretched the membrane, we used a different voltage indicator (DiSBAC2(3)[26]). As expected (Fig. 2g), reducing the stretch of the PDMS membrane quickly led to repolarization of membrane potential (Fig. 2e,f). According to the model, depolarization upon stretch is caused by a drop in cellular biomass density due to an increased cell volume, rather than tension in the plasma membrane or changes in cell-cell adhesion. Using NoRI imaging, we quantified biomass density of the confluent monolayer just before and immediately after a 20% uniaxial stretch, and then again after overnight cultivation (Fig. 2h,i). As expected from the tissue simulation (Fig. 2j), we found that stretching resulted in a significant drop in biomass density and induced biomass production and proliferation, as biomass density and cell number recovered to their initial level overnight. Conversely, we also confirmed that de-stretching the PDMS membrane resulted in an increase of cellular biomass density after overnight recovery (Fig. S7).

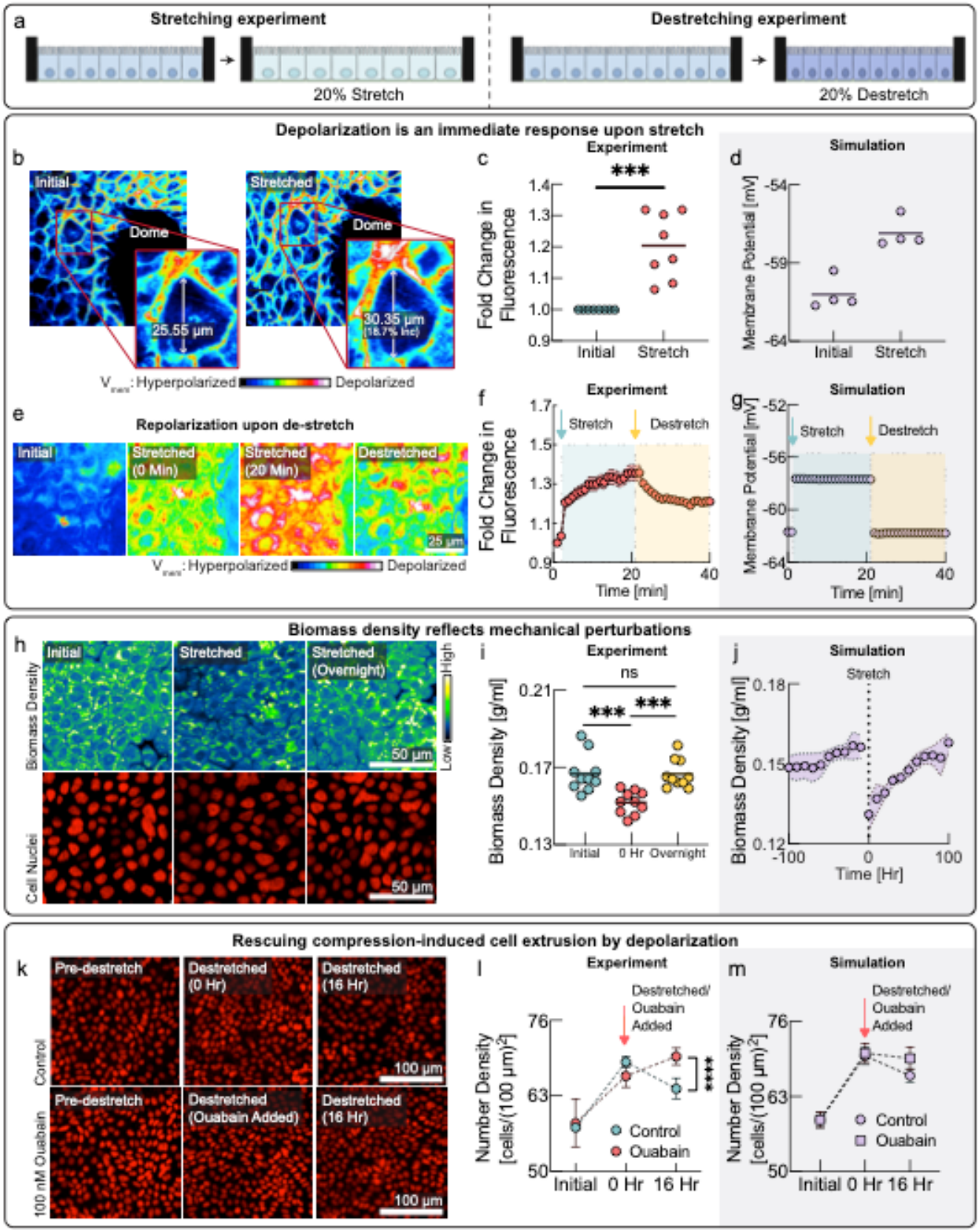

Figure 2: Cells detect and respond to mechanical forces via membrane potential. a, *Schematic diagram depicting the experimental design with cells on stretchable membrane. In one case, cells were grown to confluence and then 20% uniaxial stretch was applied (left panel) or cells*

were grown to confluence on a pre-stretched membrane, and then the stretch was released to induce compression (right panel). ***b,*** *Cells in a confluent monolayer depolarize rapidly on application of uniaxial stretch. Cells imaged in the presence of the membrane potential dye (Fluo-Volt), where an increase in fluorescence intensity indicates depolarization of membrane potential. Callout shows the increase in cellular area on stretching. Length was measured in the direction of stretch.* ***c,*** *Plot of fluorescence intensity (increase representing depolarization of membrane potential) on uniaxial stretching similar to panel b (8 cells quantified, p=0.0006, paired t-test).* ***d,*** *Membrane potential predicted by the tissue simulation upon a 20% uniaxial stretch (each point represents average from 4 independent simulations).* ***e,*** *Reversibility of membrane potential change on stretching and de-stretching using a different membrane potential indicator. Cells were grown to confluence on a stretchable PDMS membrane and loaded with membrane potential sensitive dye (DiSBAC2(3)). A 20% uniaxial stretch was applied (20%). Increase in fluorescence intensity represents depolarization on stretching. After the membrane was de-stretched, fluorescence intensity decreased quickly, indicating repolarization as compared to the stretched depolarized state. Note that for technical reasons, we cannot de-stretch back to exact same initial point.* ***f,*** *Quantification of reversibility of membrane potential on stretching and de-stretching. Increase in fluorescence intensity indicates depolarization, whereas decrease indicates hyperpolarization. Cyan arrow indicates the timepoint of stretch. Yellow arrow represents timepoint of de-stretch. Fast reversibility of depolarization of membrane potential rules out changes in permeability due to membrane stretch as the cause of depolarization. (8 cells quantified, error bars represent SD).* ***g,*** *Corresponding tissue simulation predicting depolarization and repolarization upon stretch and de-stretch.* ***h****, Response of cellular biomass to tissue stretch, measured by NoRI imaging. Biomass density of the confluent epithelial monolayer drops with uniaxial stretch. Biomass density recovers to the initial biomass density level overnight.* ***i,*** *Quantification of biomass density via NoRI imaging from same experiments as panel h. (2 independent experiments, 5 cells from each experiment. Unpaired t test, p-value, initial and 0 Hr = 0.0006, 0 Hr to overnight = 0.0001.)* ***j,*** *Tissue simulation recapitulates the drop of biomass density upon stretch and overnight recovery. (Average from 4 simulations, error bars represent SD.)* ***k,*** *Tissue crowding was induced by de-stretching of the PDMS membrane (top images). After 16h a significant number of cells had been eliminated, consistent with previous studies*[23,24]*. We show here that cells can be rescued from extrusion upon de-stretch and retained at a higher tissue density by mild depolarization (bottom images).* ***l,*** *Quantification of cell number in same experiments as panel k. Depolarization leads to cells being retained in the tissue at a significantly higher cell number density than in the control (red vs cyan data points). (20 ROIs quantified from 3 independent experiments. Error bars represent SEM. p-value <0.0001, calculated from comparing 60 ROIs of control and depolarizing conditions.)* ***m,*** *Tissue simulation recapitulates cell elimination after compression and rescue from elimination by depolarizing drugs. (Average from 4 simulations, error bars represent SEM.)*

Depolarization rescues cells from elimination after mechanical compression

We wished to directly test the role of the membrane potential in regulating the response of cells to mechanical perturbations. Therefore, we grew MDCK cells on pre-stretched membranes to high cell density and then decreased the stretch to induce cell crowding and compression of the tissue (Fig. 2k). Cell extrusion in response to tissue compression is well established[23,24]. If

crowding induced hyperpolarization plays the central role cell in determining the cell number density, it should be possible to retain a higher cell number density simply by depolarizing the tissue. As we expected, in the presence depolarizing drugs, cells maintained a significantly higher cell number density after the tissue was compressed (Fig. 2k,l red vs. blue circles). The observed experimental dynamics are consistent with our model and could be recapitulated with the tissue simulation when we simulated uniaxial compression of the tissue (Fig. 2m). In a separate experiment, we induced crowding while cells were still in growth phase and observed the same increase of steady-state cell number density when cells were treated with a different depolarizing drug, TCT[15,16] (Fig. S8).

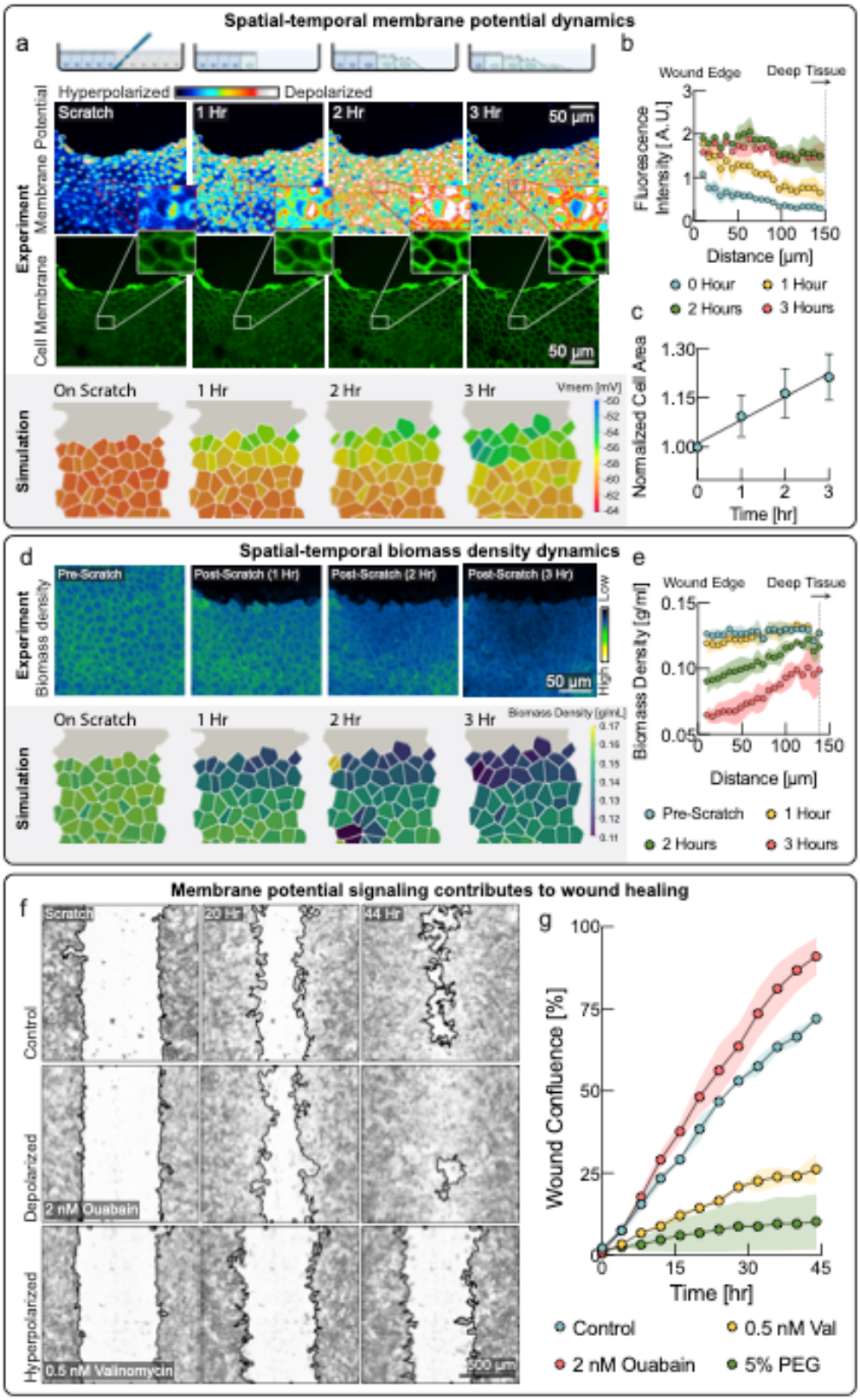

Figure 3: A mechanically induced depolarization wave enhances wound healing. a, *Upper panel: Cells progressively depolarize with time after scratch wound formation. Cells*

immediately next to the wound depolarize earlier and the depolarization wave propagate deeper in the tissue as time progresses. Membrane potential was measured via the membrane potential dye DisBac. An increase in fluorescence intensity (color scale) represents depolarization. Lower panel: Area of cells close to the wound increases with time, indicative of mechanical. Lower panel: Membrane potential from the tissue simulation over the course of wound healing. ***b****, Quantification of membrane potential as a function of distance from scratch wound at different times. (Averaged pixel values from 4 rectangular ROI of 100 µm width. Error bars represent SD.)* ***c,*** *Quantification of cell area shows expansion of cells during wound healing. (Normalized cell area quantified from 9 cells. Error bars represent SD.)* ***d,*** *Upper panel****:*** *Biomass density via NoRI imaging over the course of wound healing. Lower panel: Biomass density from the tissue simulation over the course of wound healing.* ***e.*** *Quantification of cellular biomass density as a function distance from scratch wound at different times after wounding. (Biomass density from 4 rectangular ROIs of 50 um width. Error bars represent SD.)* ***f,*** *Wound healing efficiency is modulated by changes in membrane potential. Representative microscopic images of control well, depolarizing drug treatment (ouabain) and hyperpolarizing drug treatment (valinomycin). Mild depolarization results in better wound healing, as compared to control. The improvement in wound healing speed was also found with treatment with other depolarizing drugs (Fig. S11). On the other hand, hyperpolarization severely disrupted wound healing.* ***g,*** *Quantification of wound area closed, plotted as a function of time. Depolarization resulted in faster wound healing (ouabain, red circles), as compared to the untreated control (cyan circles). Hyperpolarization (valinomycin, yellow circles) resulted in disruption of wound healing. Hyperpolarization via addition osmotic compression (5% PEG, green circles) had the same effect. (Wound confluence calculated using incucyte software, 2 independent wells, average wound confluence reported with SD.)*

Mechanical stretch results in a wave of depolarization during wound healing

To investigate a natural situation, where substantial dynamical changes in tissue density and mechanical forces are occurring, we decided to investigate wound healing. All tissues can experience injuries that must be detected and quickly repaired in a controlled fashion. During wound healing, mechanisms of tissue homeostasis are operating in high gear and mechanical regulation may play an important role. To investigate the role of membrane potential in wound healing, we performed scratch wound assays on confluent colonies of MDCK cells. Strikingly, we observed a wave of depolarization in the tissue, starting at the wound's immediate edge and moving deeper into the tissue over several hours (Fig. 3a, quantified in 3b). Depolarization at wound edges has been previously observed, but the mechanistic cause of this depolarization has yet to be explained[27,28]. According to our model, a drop of biomass density due to mechanical stretching of the tissue could explain depolarization. Indeed, we observed an increase in cell area in the tissue indicative of mechanical stretch (Fig. 3a, middle & 3c), as cells became motile via the epithelial mesenchymal transition (Fig. S9) and moved into the wound area, pulling on the cell behind them. Using NoRI imaging, we quantified biomass density as a function of distance from the wound edge (Fig. 3d, e & Fig. S10). Remarkably, we observed a drop in biomass density that closely coincided with the depolarization wave. Indeed, the tissue simulation with the mechano-electro-osmotic model successfully recapitulates the temporal and spatial dynamics of biomass density and membrane potential during wound healing (Fig. 3a, d, lower panels).

We hypothesize that the physiological function of this wave of depolarization might be to upregulate motility forces and proliferation in cells that are not immediately adjacent to the wound edge. Based on the previous experiments, this would be expected to speed up the wound healing process. Indeed, we observed both depolarization (Fig. 3a) and a drop in biomass density (Fig. S9) in cells immediately adjacent to the wound, as they underwent the epithelial-mesenchymal transition. It is also known that motility forces of cells many cell rows away from the wound generate most of the tissue tension, resulting in wound closure[29]. Thus, according to this hypothesis, cells at the immediate wound edge become motile first and move into the wound. The migration mechanically stretches cells in rows behind them. As this wave of mechanical stretch propagates deeper into the tissue, it causes a drop in biomass density, resulting in depolarization of membrane potential. Cells detecting the tissue stretching via the changed membrane potential may upregulate motility, biomass production and proliferation to enhance wound healing.

Depolarization enhances efficiency of wound healing

By applying depolarizing and hyperpolarizing drugs and quantifying wound healing speed, we tested whether modulation of the membrane potential directly affects the speed and efficiency of wound healing We used CHO cells instead of MDCK cells because MDCK tissues tended to detach entirely during scratch wounding when an automated scratch wounding device was used. Indeed, even low concentrations of hyperpolarizing drugs (valinomycin) dramatically slowed down wound healing (Fig. 3f, lower panel & Fig. 3g, yellow circles) as compared to the DMSO control. We had previously established that compression of cells by raising the external osmolarity resulted in hyperpolarization of membrane potential (Fig. S4). Indeed, compression by external osmolarity (Fig. 3g, green circles & Fig. S11) phenocopies the effect of hyperpolarizing drugs. Even more remarkably, we also found that the efficiency of wound healing could be increased, becoming faster than wild-type tissues with the addition of depolarizing drugs (Fig. 3f, middle & Fig. 3g, red circles). This is evident as compared to the untreated control (Fig.3f, upper & Fig. 3g, cyan circles). Depolarization by other drugs showed a similar improvement of wound healing efficiency (Fig. S11). These data suggest that depolarizing cells provides them with a 'head start' to upregulate motility and proliferation, as compared to the control tissue, where depolarization is only triggered later, by stretching from the other cells moving into the wound.

Membrane potential controls important mechano-transduction pathways

Our data show that membrane potential is a direct readout of mechanical forces and tissue density and plays an important role in tissue homeostasis. But how is membrane potential integrated with signal transduction pathways to mediate these phenotypes? We wondered whether membrane potential might directly affect pathways implicated in mechano-sensing such as Hippo and MAPK[30–36]. We found that the nuclear/cytoplasmic localization of the Hippo pathway downstream effector YAP is continuously modulated by tissue density (Fig. 4a-c), consistent with previous observations[37]. We hypothesized that density-dependent the modulation of YAP localization might be due to membrane potential. Strikingly, we found that depolarization alone was sufficient to make YAP re-enter the nucleus in highly confluent tissues (Fig. 4d) comparable to the ratio in cells at low confluence. Consistently, we also observed stabilization and increased level of total YAP under depolarized conditions, whereas total YAP

marginally decreased under hyperpolarization (Fig S12a). The observed regulation of YAP by membrane potential can easily be understood in the context of our physiological observations. Low tissue density results in depolarized membrane potential (Fig. 1&2), resulting in localization of YAP to the nucleus (Fig.4d), promoting cell growth and cell cycle progression [37,38]. On the other hand, high tissue density is reflected in fully polarized membrane potential (Fig. 1&2), resulting in YAP exiting the nucleus (Fig.4a-d) and suppressing proliferation.

Next, we tested the effect of membrane potential on the MAP kinase pathways. Remarkably, we found that depolarization shifted the active form of both p-p38 (p-Tyr 182) and p-JNK (p-Thr 183, p-Tyr 185) from nuclear localization to cytoplasmic localization (Fig. 4e,f). Nuclear localization of activated JNK and p38 at high tissue density may contribute to tissue homeostasis by suppressing proliferation, promoting autophagy, inducing apoptosis, or causing cell extrusion[39–41]. Reduction in the level of nuclear localized p-JNK under depolarization may promote proliferation at low tissue density.

Finally, we measured the dependence of Src signaling on membrane potential. Depolarization stabilized phosphorylated Src (Fig. S12a), while hyperpolarization strongly reduced its levels (Fig. S12a). Active Src kinase signaling can activate many downstream targets, including EGFR[42–44] , PI3K[45], and PDK1, which can stimulate proliferation and motility. The downstream cellular responses elicited by membrane-potential-mediated Src signaling are consistent with the role of membrane potential in tissue homeostasis and wound healing, shown in Figs. 1-3.

Our findings in combination with previous observations reveal possible signal transduction routes of mechano-transduction via membrane potential (Fig. 4g). K-Ras and EGFR have been previously shown to be modulated by membrane potential[46–48] and could mediate the membrane potential dependent MAPK signaling that we observe. Moreover, membrane potential controlled cytoplasmic localization of p-JNK may affect YAP nuclear localization, as p-JNK-mediated LIMD1 phosphorylation can un-sequester YAP from the LIMD1-LATS complex, promoting its nuclear translocation[49]. Thus, these interactions constitute a continuous pathway connecting mechano-dependent voltage across the plasma membrane with nuclear localization of key signaling proteins (Fig. 4g).

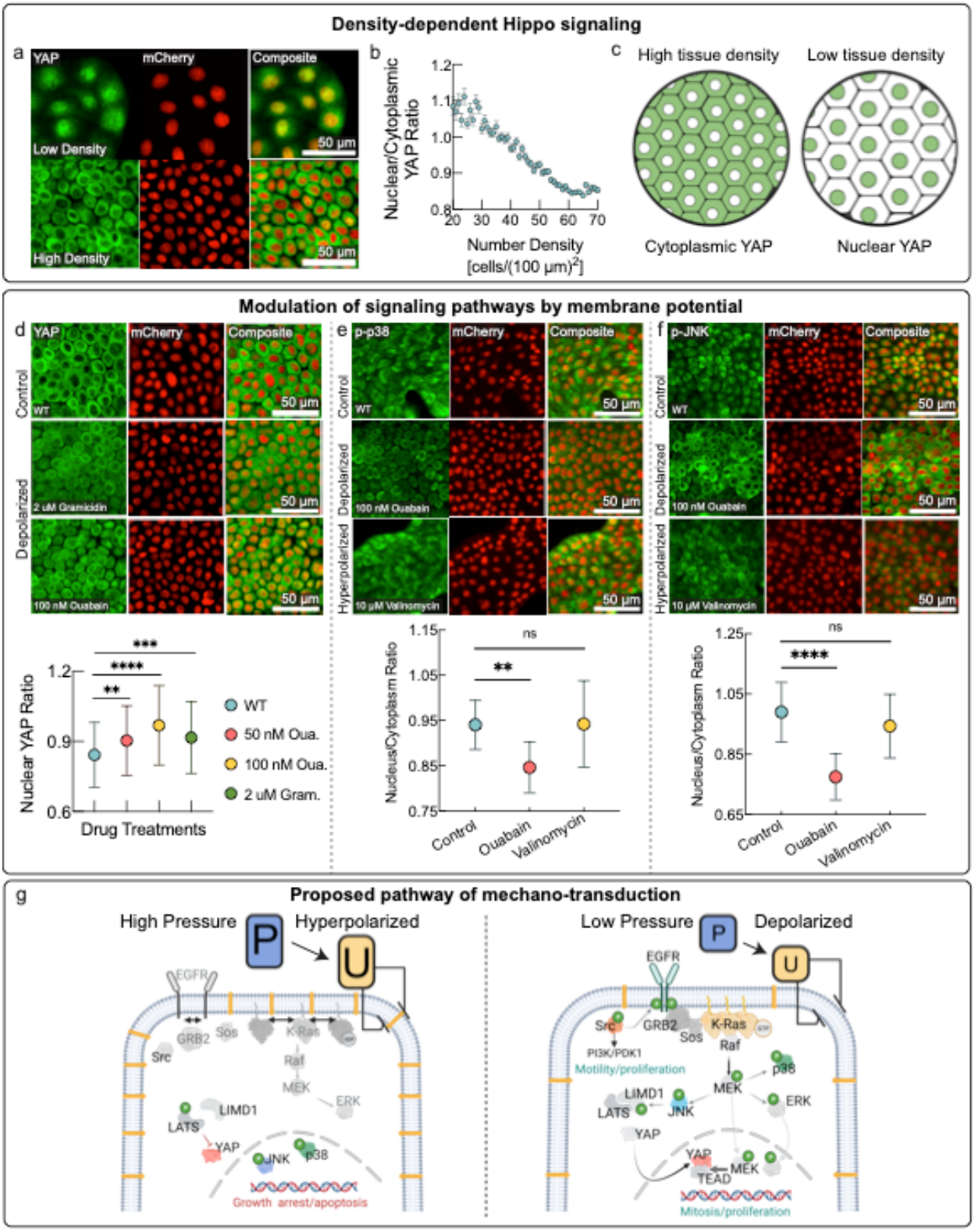

Figure 4: Membrane potential-mediated mechano-transduction pathways. a, *Localization of YAP via immunostaining in low density (top panel) and high density MDCK tissues (bottom panel).* ***b,*** *Quantification of nuclear-to-cytoplasmic YAP ratio as a function of cell number*

density. (Cells binned according to their local neighbor density with increment of 1 cells, each point represents the bin of integer number density and N represent total number of cells in that bin. Total of 20337 cells analyzed). ***c,*** *Schematic representation of YAP localization at different cell number densities. YAP is the Hippo pathway downstream effector that localizes to nucleus and promotes cell division in sub-confluent cells, whereas YAP is excluded from the nucleus in confluent cells, decreasing the rate of proliferation.* ***d,*** *Depolarization promotes YAP re-entry in confluent MDCK cells. YAP is excluded from the cell nuclei in untreated confluent monolayers (top). YAP re-enters nuclei on depolarization by either gramicidin (middle) or ouabain (lower). Quantification of nuclear YAP ratio (plot below). YAP localization in depolarized, high-density tissues is comparable to sub-confluent cells (as quantified in panel b). (100 cells quantified for each condition. p-value wt to 50nM ouabain is 0.0032, wt to 100 nM ouabain is <0.0001 and WT to gramicidin is 0.0005.)* ***e,*** *Membrane potential dependence of localization of phosphorylated p38 from immunostaining. Phosphorylated p38 localizes to cell nuclei in dense tissues. Depolarization by ouabain resulted in nuclear exclusion of phosphorylated p38. Hyperpolarization by valinomycin resulted in uniform distribution of phosphorylated p38 in cell nuclei and cytoplasm. Nuclear to cytoplasmic ratio of phosphorylated p38 is quantified in plot below. (10 cells quantified, p-value control to ouabain is 0.0013.)* ***f,*** *Membrane potential dependence of localization of phosphorylated JNK from immunostaining. Depolarization via ouabain caused nuclear exclusion and increased cytoplasmic localization of phosphorylated JNK (middle), whereas the untreated control (top), as well as hyperpolarization via valinomycin (bottom) exhibited uniform distribution between nuclei and cytoplasm. Quantification of nuclear to cytoplasmic ratio of phosphorylated JNK shown in plot below. (10 cells quantified, p-value control to ouabain is <0.0001)* ***g,*** *Signaling routes of mechano-transduction via membrane potential. Mechanical pressure is directly reflected in membrane potential. EGFR and K-Ras are directly exposed to the electric field across the plasma membrane resulting from membrane potential and have been previously shown to be modulated by membrane potential* [46,48,50]*. EGFR signaling can also be modulated by Src* [42–44]*, which our data shows to be under control by membrane potential (Fig. S12). We show that JNK, p38, YAP and Src signaling are also controlled by membrane potential. MAP kinases pathways are downstream from EGFR and K-Ras. JNK in turn, can affect the localization of YAP via LIMD1* [49]*. Together these interactions constitute a continuous mechano-transduction pathway connecting mechanical pressure on the cell to nuclear signaling.*

Discussion

Regulation by membrane potential can convey the size, density, and the general mechanical state of a cell. These global cellular variables are of central physiological importance for homeostasis and development, but such cell-scale properties are difficult for cells to accurately assess from local protein interactions, such as cell-cell adhesion or even stretch-activated ion channels in the plasma membrane. Membrane potential on the other hand, provides a quasi-instantaneous, globally integrated readout of cell state. The coupling between mechanical pressure, density and membrane potential is based only on elementary physical laws, requires no active regulation, and is present even in thermodynamic equilibrium, where it is known as the Gibbs-Donnan effect [12]. Therefore, even primitive cells, lacking active transport and confined by a simple cell wall, could have utilized membrane potential as a readout of their mechanical state and biomass concentration. Membrane-potential-mediated mechano-transduction may therefore have been among the first homeostatic mechanisms to emerge in multicellular organisms.

Note that while we assumed the absence of active regulation or amplification of membrane potential in our model as a proof-of-concept, there are many ways how cells could further enhance the changes in membrane potential to reflect even small differences in density and mechanical forces. We believe it is likely that rather than fixing membrane potential to a constant homeostatic value (like body temperature in mammals), which would result in a loss of the valuable information conveyed by membrane potential, cells may have evolved to actively enhance the signal-to-noise ratio of membrane potential signaling of mechanical pressure. Indeed, observed changes in membrane potential are sometimes even larger than those expected from our model without signal amplification (Fig. S3).

Note also that while we have shown that several important mechano-transduction pathways are controlled by membrane potential, there are likely other parallel signal transduction routes that are affected by membrane potential. Calcium signaling would be an ideal effector of membrane-potential-mediated mechano-transduction. This could occur either via voltage-gated channels in the plasma membrane and the strong voltage-dependence of equilibrium calcium concentration that results from the calcium ion's two positive charges. Indeed, flux through key calcium channels like Piezo has been shown to strongly depend on membrane potential[51] and Piezo has been shown to be voltage-gated[52].

The concept of mechano-sensing via membrane potential should not be thought of as limited to epithelia or even multi-cellular tissues. For instance, stem cell differentiation has been shown to depend on both cell volume and osmotic pressure[53,54], as well as membrane potential[55], suggesting a role of membrane-potential-mediated mechanical signaling. As another example, the response of membrane potential to cellular compression may play a role in neuronal mechano-transduction if mechanical forces affect total neuronal cell volume. The resulting changes in resting membrane potential could trigger voltage-gated channels and calcium siganling[51,52].

Finally, the importance of membrane potential in tissue growth control that we observe, suggests that mis-regulation of membrane potential or its downstream signaling cascade could have dramatic consequences for tissue homeostasis, potentially resulting in tumorigenesis when cells stop responding to the mechanical cues from their environment. In fact, this may explain the frequent occurrence of ectopic expression of neuronal ion channels in tumors[56] and the commonly observed phenotype of depolarized resting membrane potential in cancer[57].

Acknowledgements
We would like to thank Sean Megason, Tim Mitchison, Jan Skotheim, and Xavier Trepat for their comments and feedback on the manuscript. We would like to thank Peter Sorger and Clarance Yapp for access to their high content imaging systems. Thanks to Eugenia Piddini (University of Bristol), J.J. Fredberg and C.Y. Park (Harvard T.H. Chan School of Public Health) for helping us with MDCK cells. We thank Nikon imaging center at Harvard Medical School for help with all fluorescence imaging experiments. Specifically, we thank Jennifer Waters, Tally Lambert, Anna Payne-Tobin Jost for their valuable support with the microscopy. This project was supported by MIRA grant (5R35GM137895) and an HMS Junior Faculty Armenise grant to M.B. N.C.B was supported by following grants National Science Foundation Graduate Research

Fellowship Program (DGE 2140743) and Systems, Synthetic, and Quantitative Biology Training grant award (T32GM135014). Any opinions, findings, and conclusions or recommendations expressed in this material are those of the author(s) and do not necessarily reflect the views of the National Science Foundation.

References

1. *Molecular Biology of the Cell: Reference edition, Band 1*. (2008).
2. Hille, B. Ion channels of excitable membranes. in (2001).
3. Panciera, T., Azzolin, L., Cordenonsi, M. & Piccolo, S. Mechanobiology of YAP and TAZ in physiology and disease. *Nat Rev Mol Cell Biol* **18**, 758–770 (2017).
4. Niisato, N., Post, M., Van Driessche, W. & Marunaka, Y. Cell Swelling Activates Stress-Activated Protein Kinases, p38 MAP Kinase and JNK, in Renal Epithelial A6 Cells. *Biochem Biophys Res Commun* **266**, 547–550 (1999).
5. Kishi, H. *et al*. Osmotic Shock Induces G1 Arrest through p53 Phosphorylation at Ser33 by Activated p38MAPK without Phosphorylation at Ser15 and Ser20. *Journal of Biological Chemistry* **276**, 39115–39122 (2001).
6. Lee, S.-H., Park, Y., Yoon, S. K. & Yoon, J.-B. Osmotic Stress Inhibits Proteasome by p38 MAPK-dependent Phosphorylation. *Journal of Biological Chemistry* **285**, 41280–41289 (2010).
7. HuangFu, W.-C., Omori, E., Akira, S., Matsumoto, K. & Ninomiya-Tsuji, J. Osmotic Stress Activates the TAK1-JNK Pathway While Blocking TAK1-mediated NF-κB Activation. *Journal of Biological Chemistry* **281**, 28802–28810 (2006).
8. Buckley, C. E. & St Johnston, D. Apical–basal polarity and the control of epithelial form and function. *Nat Rev Mol Cell Biol* **23**, 559–577 (2022).
9. Oh, S. *et al.* Protein and lipid mass concentration measurement in tissues by stimulated Raman scattering microscopy. *Proc Natl Acad Sci U S A* **119**, e2117938119 (2022).
10. Park, H. *et al.* Three-dimensional refractive index tomograms and deformability of individual human red blood cells from cord blood of newborn infants and maternal blood. *https://doi.org/10.1117/1.JBO.20.11.111208* **20**, 111208 (2015).
11. Shin, S., Kim, K., Yoon, J. & Park, Y. Active illumination using a digital micromirror device for quantitative phase imaging. *Optics Letters, Vol. 40, Issue 22, pp. 5407-5410* **40**, 5407–5410 (2015).
12. Donnan, F. G. Theorie der Membrangleichgewichte und Membranpotentiale bei Vorhandensein von nicht dialysierenden Elektrolyten. Ein Beitrag zur physikalisch-chemischen Physiologie. *Zeitschrift für Elektrochemie und angewandte physikalische Chemie* **17**, 572–581 (1911).
13. Abdelfattah, A. S. *et al.* Bright and photostable chemigenetic indicators for extended in vivo voltage imaging. *Science (1979)* **365**, 699–704 (2019).
14. Cone, C. D. & Tongier, M. Contact inhibition of division: involvement of the electrical transmembrane potential. *J Cell Physiol* **82**, 373–86 (1973).
15. Barboiu, M. *et al.* Polarized Water Wires under Confinement in Chiral Channels. *J Phys Chem B* **119**, 8707–8717 (2015).
16. Barboiu, M. *et al.* An artificial primitive mimic of the Gramicidin-A channel. *Nat Commun* **5**, 4142 (2014).

17. Goldman, D. E. POTENTIAL, IMPEDANCE, AND RECTIFICATION IN MEMBRANES. *J Gen Physiol* **27**, 37 (1943).
18. TOSTESON, D. C. & HOFFMAN, J. F. Regulation of Cell Volume by Active Cation Transport in High and Low Potassium Sheep Red Cells. *Journal of General Physiology* **44**, 169–194 (1960).
19. Kay, A. R. & Blaustein, M. P. Evolution of our understanding of cell volume regulation by the pump-leak mechanism. *Journal of General Physiology* **151**, 407–416 (2019).
20. Armstrong, C. M. The Na/K pump, Cl ion, and osmotic stabilization of cells. *Proceedings of the National Academy of Sciences* **100**, 6257–6262 (2003).
21. Dyer, K. F. The Quiet Revolution: A New Synthesis of Biological Knowledge. *J Biol Educ* **5**, 15–24 (1971).
22. Milo, R., Jorgensen, P., Moran, U., Weber, G. & Springer, M. BioNumbers—the database of key numbers in molecular and cell biology. *Nucleic Acids Res* **38**, D750 (2010).
23. Eisenhoffer, G. T. & Rosenblatt, J. Bringing balance by force: live cell extrusion controls epithelial cell numbers. *Trends Cell Biol* **23**, 185–192 (2013).
24. Eisenhoffer, G. T. *et al.* Crowding induces live cell extrusion to maintain homeostatic cell numbers in epithelia. *Nature* **484**, 546–549 (2012).
25. Park, J. *et al.* Screening fluorescent voltage indicators with spontaneously spiking HEK cells. *PLoS One* **8**, (2013).
26. Burgstahler, R. *et al.* Confocal ratiometric voltage imaging of cultured human keratinocytes reveals layer-specific responses to ATP. *Am J Physiol Cell Physiol* **284**, (2003).
27. Chifflet, S. *et al.* Early and late calcium waves during wound healing in corneal endothelial cells. *Wound Repair and Regeneration* **20**, 28–37 (2012).
28. Reid, B. & Zhao, M. The Electrical Response to Injury: Molecular Mechanisms and Wound Healing. *Adv Wound Care (New Rochelle)* **3**, 184–201 (2014).
29. Trepat, X. *et al.* Physical forces during collective cell migration. *Nat Phys* **5**, 426–430 (2009).
30. Chang, Y. C., Wu, J. W., Wang, C. W. & Jang, A. C. C. Hippo Signaling-Mediated Mechanotransduction in Cell Movement and Cancer Metastasis. *Front Mol Biosci* **6**, 157 (2020).
31. HuangFu, W.-C., Omori, E., Akira, S., Matsumoto, K. & Ninomiya-Tsuji, J. Osmotic Stress Activates the TAK1-JNK Pathway While Blocking TAK1-mediated NF- B Activation: TAO2 REGULATES TAK1 PATHWAYS. *Journal of Biological Chemistry* **281**, 28802–28810 (2006).
32. Lee, S.-H., Park, Y., Yoon, S. K. & Yoon, J.-B. Osmotic stress inhibits proteasome by p38 MAPK-dependent phosphorylation. *J Biol Chem* **285**, 41280–9 (2010).
33. Kishi, H. *et al.* Osmotic shock induces G1 arrest through p53 phosphorylation at Ser33 by activated p38MAPK without phosphorylation at Ser15 and Ser20. *J Biol Chem* **276**, 39115–22 (2001).
34. Messaoud, N. ben, Katzarova, I. & López, J. M. Basic Properties of the p38 Signaling Pathway in Response to Hyperosmotic Shock. doi:10.1371/journal.pone.0135249.
35. Niisato, N., Post, M., van Driessche, W. & Marunaka, Y. Cell Swelling Activates Stress-Activated Protein Kinases, p38 MAP Kinase and JNK, in Renal Epithelial A6 Cells. *Biochem Biophys Res Commun* **266**, 547–550 (1999).
36. Dupont, S. *et al.* Role of YAP/TAZ in mechanotransduction. *Nature* **474**, 179–183 (2011).

37. Benham-Pyle, B. W., Pruitt, B. L. & Nelson, W. J. Mechanical strain induces E-cadherin–dependent Yap1 and β-catenin activation to drive cell cycle entry. *Science (1979)* **348**, 1024–1027 (2015).
38. Piccolo, S., Dupont, S. & Cordenonsi, M. The biology of YAP/TAZ: Hippo signaling and beyond. *Physiol Rev* **94**, 1287–1312 (2014).
39. Zeke, A., Misheva, M., Reményi, A. & Bogoyevitch, M. A. JNK Signaling: Regulation and Functions Based on Complex Protein-Protein Partnerships. *Microbiol Mol Biol Rev* **80**, 793 (2016).
40. Maik-Rachline, G., Lifshits, L. & Seger, R. Nuclear P38: Roles in Physiological and Pathological Processes and Regulation of Nuclear Translocation. *International Journal of Molecular Sciences 2020, Vol. 21, Page 6102* **21**, 6102 (2020).
41. Dhanasekaran, D. N. & Reddy, E. P. JNK signaling in apoptosis. *Oncogene* **27**, 6245–6251 (2008).
42. Stover, D. R., Becker, M., Liebetanz, J. & Lydon, N. B. Src Phosphorylation of the Epidermal Growth Factor Receptor at Novel Sites Mediates Receptor Interaction with Src and P85α. *Journal of Biological Chemistry* **270**, 15591–15597 (1995).
43. Tice, D. A., Biscardi, J. S., Nickles, A. L. & Parsons, S. J. Mechanism of biological synergy between cellular Src and epidermal growth factor receptor. *Proceedings of the National Academy of Sciences* **96**, 1415–1420 (1999).
44. Maa, M. C., Leu, T. H., McCarley, D. J., Schatzman, R. C. & Parsons, S. J. Potentiation of epidermal growth factor receptor-mediated oncogenesis by c-Src: implications for the etiology of multiple human cancers. *Proceedings of the National Academy of Sciences* **92**, 6981–6985 (1995).
45. Beadnell, T. C. *et al.* Src-mediated regulation of the PI3K pathway in advanced papillary and anaplastic thyroid cancer. *Oncogenesis* **7**, 23 (2018).
46. Zhou, Y. *et al.* Membrane potential modulates plasma membrane phospholipid dynamics and K-Ras signaling. *Science (1979)* **349**, 873–876 (2015).
47. Bartel, D. P., Sheng, M., Lau, L. F. & Greenberg, M. E. Growth factors and membrane depolarization activate distinct programs of early response gene expression: dissociation of fos and jun induction. *Genes Dev* **3**, 304–313 (1989).
48. Wang, Y. *et al.* Regulation of EGFR nanocluster formation by ionic protein-lipid interaction. *Cell Res* **24**, 959–976 (2014).
49. Codelia, V. A., Sun, G. & Irvine, K. D. Regulation of YAP by Mechanical Strain through Jnk and Hippo Signaling. *Current Biology* **24**, 2012–2017 (2014).
50. Rosen, L. Membrane depolarization and calcium influx stimulate MEK and MAP kinase via activation of Ras. *Neuron* **12**, 1207–1221 (1994).
51. Coste, B. *et al.* Piezo1 and Piezo2 are essential components of distinct mechanically activated cation channels. *Science (1979)* **330**, 55–60 (2010).
52. Moroni, M., Servin-Vences, M. R., Fleischer, R., Sánchez-Carranza, O. & Lewin, G. R. Voltage gating of mechanosensitive PIEZO channels. *Nature Communications 2018 9:1* **9**, 1–15 (2018).
53. Guo, M. *et al.* Cell volume change through water efflux impacts cell stiffness and stem cell fate. *Proc Natl Acad Sci U S A* **114**, E8618–E8627 (2017).
54. Fan, Y. L., Zhao, H. C. & Feng, X. Q. Hypertonic pressure affects the pluripotency and self-renewal of mouse embryonic stem cells. *Stem Cell Res* **56**, 102537 (2021).

55. Levin, M. Leading Edge Bioelectric signaling: Reprogrammable circuits underlying embryogenesis, regeneration, and cancer. *Cell* **184**, 1971–1989 (2021).
56. Li, M. & Xiong, Z. G. Ion channels as targets for cancer therapy. *Int J Physiol Pathophysiol Pharmacol* **3**, 156 (2011).
57. Yang, M. & Brackenbury, W. J. Membrane potential and cancer progression. *Front Physiol* **4**, (2013).